

PUBLISHED VERSION

1. Hargreaves, Leigh Randall; Lohmann, Birgit; Winstead, C.; McKoy, V. [Elastic scattering of intermediate-energy electrons from C₆₀ molecules](#) Physical Review A, 2010; 82(6):062716

© 2010 American Physical Society

<http://link.aps.org/doi/10.1103/PhysRevA.82.062716>

PERMISSIONS

<http://publish.aps.org/authors/transfer-of-copyright-agreement>

“The author(s), and in the case of a Work Made For Hire, as defined in the U.S. Copyright Act, 17 U.S.C.

§101, the employer named [below], shall have the following rights (the “Author Rights”):

[...]

3. The right to use all or part of the Article, including the APS-prepared version without revision or modification, on the author(s)' web home page or employer's website and to make copies of all or part of the Article, including the APS-prepared version without revision or modification, for the author(s)' and/or the employer's use for educational or research purposes.”

19th March 2013

<http://hdl.handle.net/2440/63074>

Elastic scattering of intermediate-energy electrons from C₆₀ moleculesL. R. Hargreaves,¹ B. Lohmann,¹ C. Winstead,² and V. McKoy²¹*ARC Centre for Antimatter-Matter Studies, University of Adelaide, Adelaide, 5005, Australia*²*A. A. Noyes Laboratory for Chemical Physics, California Institute of Technology, Pasadena, California 91125, USA*

(Received 11 November 2010; published 30 December 2010)

Experimental and calculated differential cross sections for elastic scattering of electrons by C₆₀ molecules at collision energies of 100 to 500 eV are reported. The elastic differential cross sections were measured in a standard crossed-beam apparatus, while the calculations were performed employing the Schwinger multichannel technique at the static-exchange level. Diffraction effects, some due to the overall spherical-cage structure and some to scattering by individual C atoms, are observed in both the measured and calculated cross sections.

DOI: [10.1103/PhysRevA.82.062716](https://doi.org/10.1103/PhysRevA.82.062716)

PACS number(s): 34.80.Bm

I. INTRODUCTION

Interactions between electrons and fullerenes, crucial to understanding their fundamental chemical and physical properties, are currently of considerable interest due to the pivotal role these molecules are expected to play in the development of new nanomaterials such as carbon nanotubes [1]. Much of this attention has been directed toward the C₆₀ molecule, one of the most basic fullerene structures. Such attention has been primarily directed toward studies of excitation [2–5], electron attachment [6–9], and ionization [10–14].

Studies of more fundamental electron collision processes such as elastic scattering, however, remain limited. At low energies the only current experimental study of elastic scattering is that of Tanaka *et al.* [15], who measured relative differential cross sections (DCSs) at a single scattering angle (30°) and over a limited range of energies (1–11.5 eV). Mid- to high-incident-energy elastic interactions with C₆₀ have received some attention within the Born approximation [16–18], in general applying a quite simple spherical potential model of the C₆₀ molecule. More rigorous theoretical studies of elastic scattering were undertaken by Gianturco, Lucchese, and Sanna [19–21] and Winstead and McKoy [22]. The latter employed the Schwinger multichannel (SMC) method within the static-exchange approximation at energies up to 50 eV and observed oscillatory effects in the DCSs which were attributed to interference effects arising from Bragg-type diffraction of the incident electrons by the molecular C₆₀ cage.

Here, the earlier study of Winstead and McKoy [22] is extended to higher energies (100–500 eV). Results are calculated employing the SMC method within the static-exchange approximation, as well as with two simple models: a spherical potential shell and independent scattering from carbon atoms treated within the first Born approximation. The calculated DCSs are compared to measurements obtained using a crossed-beam apparatus.

II. EXPERIMENTAL DETAILS

With two notable exceptions, most aspects of the apparatus used for the present measurements have been described at length previously [23]. In summary, the apparatus comprised a stainless-steel high-vacuum chamber which housed a standard electron gun, electron detector, and an oven which produced

a beam of gas-phase C₆₀ molecules. The electron gun incorporated a thoriated tungsten filament source producing electrons by thermionic emission. These emitted electrons were focused into a collimated beam by a pair of three-element cylindrical-geometry lenses and steered onto the gas beam by two pairs of X-Y deflectors. The energy of the electron beam could be set up to 2000 eV and the gun produced beam currents of up to 10 μA, as measured by a Faraday cup. The energy width of the electron beam was approximately 0.5 eV, due to the thermal spread of the electrons leaving the filament. This electron beam was crossed with a gas beam of C₆₀ molecules to establish the interaction region. Electrons scattered by the gas beam were collected by an electron detector mounted onto a rotatable turntable. The turntable allowed the detector to be placed at any angle between 15° and 135° with respect to the incident beam direction. The angular range of the detector was limited by the relative positions of the Faraday cup and the electron gun. Electrons entering the detector passed through a hemispherical energy selector where they were filtered according to their energy. Elastically scattered electrons passed through the selector and impacted onto a standard channel electron multiplier (CEM). The overall energy resolution of the system was approximately 0.8 eV. Output pulses from the CEM were registered by standard counting electronics. The entire experiment was performed under computer control. For completeness, we note that the apparatus also contained a second, independently rotatable, electron detector which was identical to the one just described. The second detector was present in the system as the apparatus is normally employed for coincidence electron ionization, or (*e*,2*e*), studies; however, this detector was not used for the present measurements.

The system was modified from its previously reported configuration in order to produce a gas-phase C₆₀ beam, and these modifications are described here in slightly more detail. The major modification was the inclusion of an oven source, which produced the C₆₀ beam by vaporizing a sample of solid C₆₀ powder (Sigma-Aldrich, 98% purity). This oven comprised a stainless-steel cylindrical crucible containing the sample, which was heated by a dual-core heating element (Thermocoax), wrapped around the oven's girth, to a temperature of 450°C. The vaporized C₆₀ exited the top of the oven and was formed into a collimated gas beam by a 15-mm-long and 1.5-mm-diameter nozzle. The tip of the nozzle sat 5 mm below the electron interaction region. The

nozzle was itself independently heated to a temperature of 550°C by a second dual-core heating element to prevent C₆₀ condensing in the nozzle and blocking it. The temperature of the oven and the nozzle were separately monitored by two K-type thermocouple wires. The voltage signal from each thermocouple was amplified (LabJack LJTICK-InAmp) and fed into a 10 bit, 0–5 V analog input (LabJack U3-HV) which was, in turn, connected via a USB interface to the control PC. The temperature of both the oven and nozzle were continuously logged by the PC during the experiment. The heating elements were each powered by independent, computer-programmable, 100 W dc power supplies (B&K Precision 1786B and 1787B, respectively). The temperature of the oven was thermostatically controlled by the PC, using software written in-house under a LABVIEW 8.5 platform. The control software employed a conventional proportional-integral-derivative (PID) feedback control loop which enabled dynamic adjustments to each heater's power in order to maintain a constant temperature. The thermostat held both temperatures within $\pm 0.5^\circ\text{C}$ of their set temperature.

A cold finger was also added to condense the emitted C₆₀ and prevent it from coating the electron optics. The cold finger comprised a 7.5-cm-diameter and 41-cm-long hollow stainless-steel cylinder, which was mounted vertically above the oven off of a 6 in. ConFlat flange. The cold finger extended into the chamber to approximately 5 cm above the oven. The cold finger was filled with liquid nitrogen decanted from a 50 l Dewar. Filling of the cold finger was automated by employing two K-type thermocouple wires to act as level sensors (upper and lower). Both thermocouples were connected to the PC via LabJack amplifiers and analog input (in an identical fashion to the oven's thermocouples). The PC filled the cold finger as necessary by operating a two-way 24 V dc cryogenic solenoid valve (ASCO), using a 5 V digital output (LabJack U3-HV) driving an electrical relay to control the valve. Filling was initiated when the lower sensor was no longer immersed in the liquid (i.e., recorded a temperature higher than liquid nitrogen temperature) and ceased when the upper-level sensor was immersed in the liquid. The control software for the autofiller was again written in-house in LABVIEW 8.5.

III. COMPUTATIONAL DETAILS

Cross sections for elastic scattering of 100 to 500 eV electrons by C₆₀ were calculated using the SMC method within the static-exchange approximation (that is, treating the electron density of the molecule as frozen throughout the collision and thus omitting polarization, excitation, and ionization). Details of the calculations are the same as in previously reported work at lower collision energies [22]. However, in order to obtain converged results at the energies of present interest, larger angular quadratures were employed in computing the on-shell component of the free-electron Green's function and the elastic scattering amplitude as a function of scattering angle. Convergence at a given energy was checked by enlarging the quadrature until the changes became negligible.

To assist in understanding the results, differential cross sections were also computed using two simple one-electron models. The first, also considered in previous work [22], treats

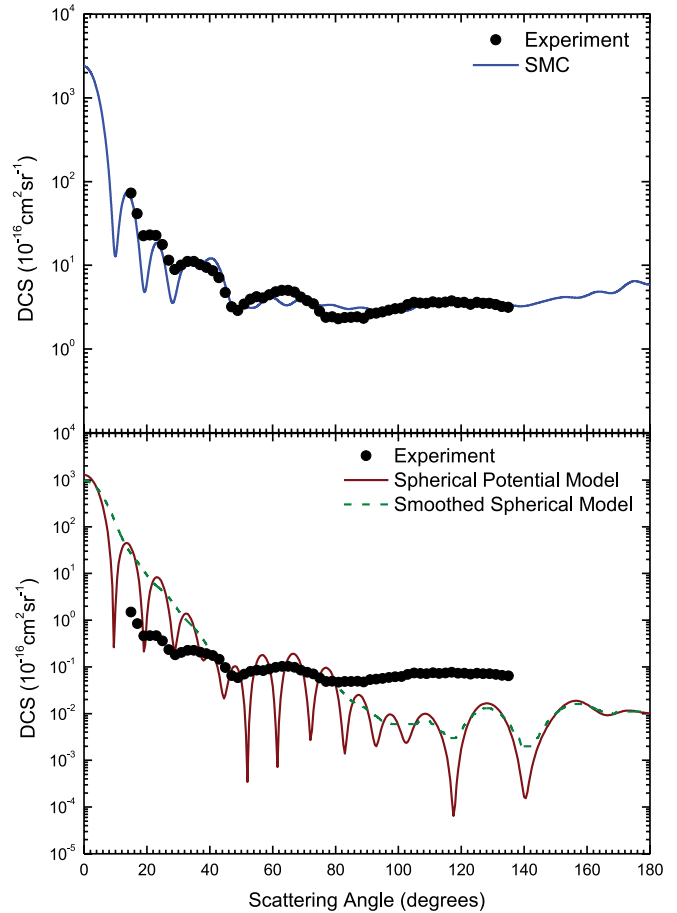


FIG. 1. (Color online) Elastic DCSs for C₆₀ molecules, at an incident energy of 100 eV. The upper panel shows the present experimental data compared with the results of the full SMC calculation. The lower panel shows the same experimental data compared with calculated results employing a spherical potential model, and the same spherical potential calculation convolved with a 5° FWHM Gaussian.

C₆₀ as nothing more than a spherical shell of attractive potential whose thickness and depth are determined, respectively, by the covalent radius of C and the electron affinity of C₆₀. Despite its simplicity, this model was found to be remarkably successful at predicting the locations of low-energy shape resonances [22]. The second model, appropriate for high-energy collisions, treats the molecule as 60 independent, identical scattering centers within the first Born approximation (independent-atom model, IAM). In this model, the elastic DCS reduces to the first Born elastic cross section of the C atom times a coefficient $A(\mathbf{q})$ given by

$$A(\mathbf{q}) = N + \sum \sum 2 \cos[\mathbf{q}(\mathbf{R}_i - \mathbf{R}_j)], \quad (1)$$

where N is the number of scattering centers (here 60), \mathbf{R}_i is the position of the i th center, and the double sum runs over all unique (i, j) pairs. $A(\mathbf{q})$ is a function of the momentum transfer $\mathbf{q} = \mathbf{k}_i - \mathbf{k}_f$, where \mathbf{k}_i and \mathbf{k}_f are the initial and final wave vectors, and thus for elastic scattering depends only on the collision energy $E (=k^2/2$, in atomic units, where

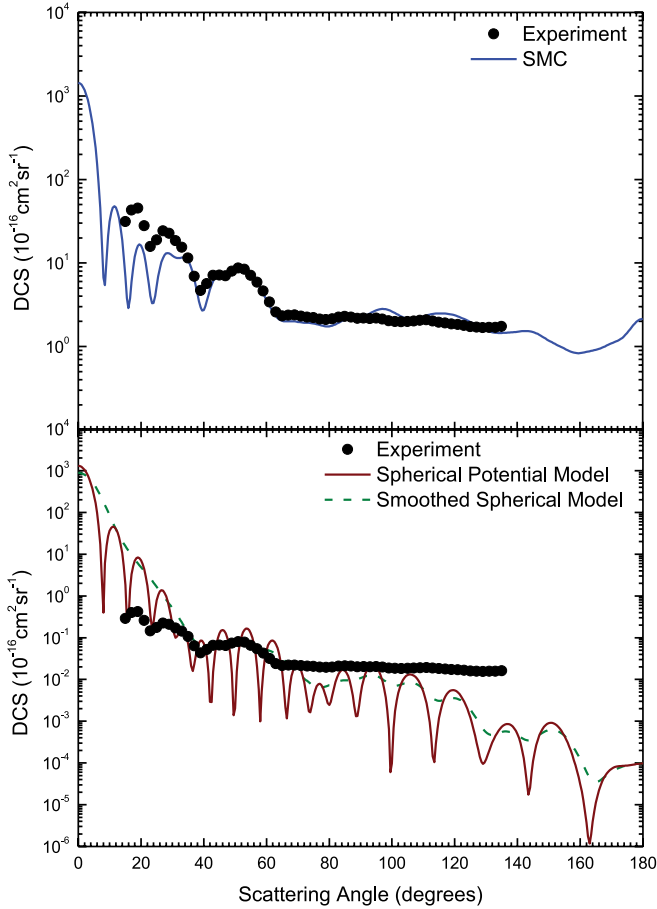


FIG. 2. (Color online) As for Fig. 1, but at an incident energy of 150 eV.

$k = |\mathbf{k}_i| = |\mathbf{k}_f|$) and on the scattering angle θ , via

$$|\mathbf{q}|^2 = 2k^2 [1 - \cos(\theta)]. \quad (2)$$

To compare with gas-phase data, the above expression for $A(\mathbf{q})$ was averaged over orientations of the molecule with respect to the axis system in which \mathbf{q} is defined to yield a value $A(q)$ that depends only on the magnitude $q = |\mathbf{q}|$ of the momentum transfer. The Born cross section of the carbon atom was evaluated from the electron scattering factor using the eight-parameter fit of Peng [24].

IV. RESULTS

The present elastic DCS results are shown in Figs. 1–6. The experimental values are relative; absolute values for the cross sections were not determined in these measurements as the system was not configured to allow implementation of the relative flow technique [25]. Instead, the experimental data points are normalized to the calculated results at the broad peak located at scattering angle around 30°–45° in each of the data sets, to allow for a comparison of the shape of the DCSs. In the absence of any absolute normalization, the uncertainties on the experimental data contain only counting statistics, which in most instances are smaller than the point markers in the figures. Also shown in the figures are the calculated

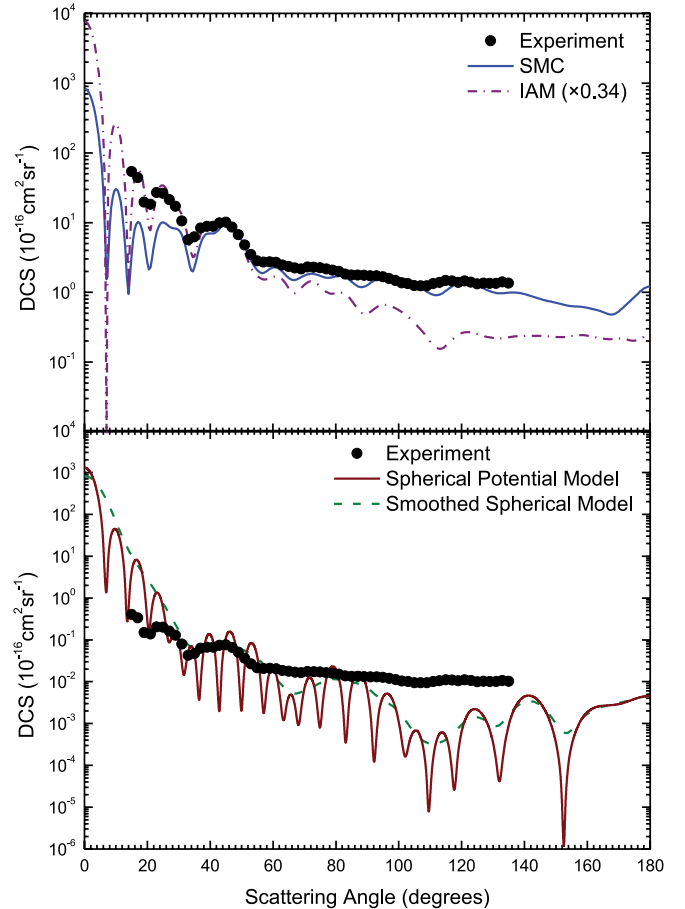


FIG. 3. (Color online) As for Fig. 1, but at an incident energy of 200 eV. Results from the IAM calculation, scaled onto the SMC data, are also shown. The scaling factor is indicated in the figure.

results employing the SMC method and both one-electron models.

At the lower energies the present experimental results are in good accord with the data from the full SMC calculation. In particular, the diffraction minima in the forward scattering portion of the cross section observed in the experimental data are predicted by the SMC model, with the locations of these oscillations well described. At high energies the SMC calculation may be expected to underestimate the forward peak, which is sensitive to very high partial waves, and overestimate the DCS at intermediate to high angles. This trend is observed in the comparison with the experimental data: the present SMC results are less forward peaked than the experimental results at all energies considered, with the possible exception of 100 eV. The description of the mid- to back-angle scattering is good at energies of 200 eV or less, but at higher energies the experimental results decrease in the mid- to backward scattering angles more rapidly than predicted by the SMC calculation.

While the experimental results show an increasing discrepancy with the SMC data as the incident energy is raised, the spherical potential model shows the opposite trend. This is highlighted in Figs. 1–6 by showing the results of the spherical potential calculation, and the result from the same calculation convolved with a 5° full width at half maximum

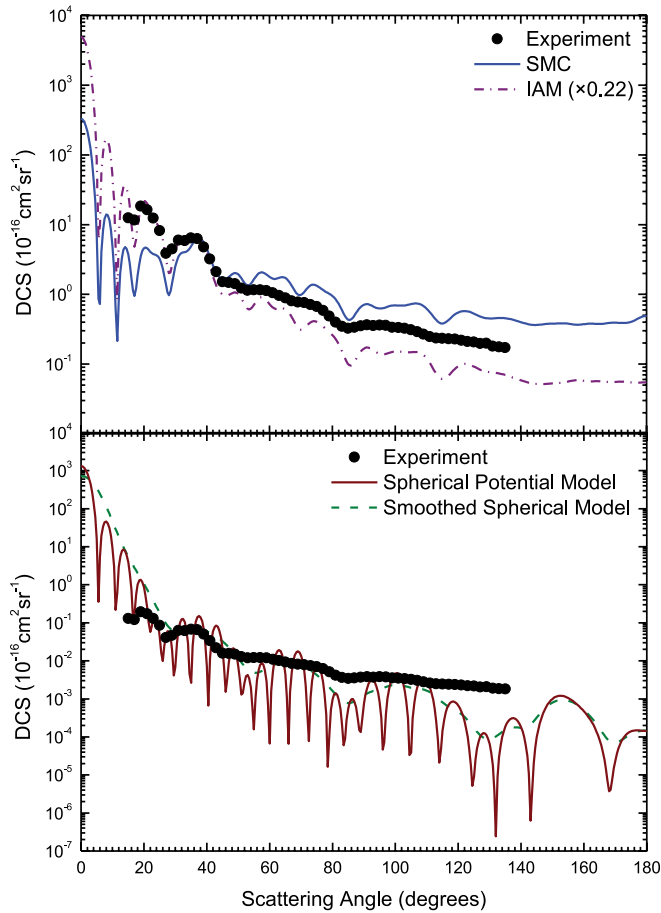


FIG. 4. (Color online) As for Fig. 3, but at an incident energy of 300 eV.

(FWHM) Gaussian to smooth out the Mie-type fringes that are artifacts of the model. As noted, at lower energies the simple spherical potential model gave a remarkably good description of the diffraction structures in the cross section, at least in the forward scattering direction [22]. At the energies considered here the Mie fringes, and the subsequent smoothing procedure, obscure any such fine structure in the cross section. The spherical potential model therefore does not observe the diffraction effects seen in the experiment and full SMC calculation. However, at incident energies greater than 300 eV the smoothed model does give a better description of the overall DCS structure than the SMC data, particularly at intermediate to high scattering angles.

The results of the IAM, which considers the molecule as 60 independent scattering centers, are shown at 200, 300, 400, and 500 eV in Figs. 3–6. The IAM results are, in general, larger in magnitude than the SMC data in the forward direction and drop off more rapidly in the backward direction. The IAM results in the figures have been scaled onto the SMC data, at the same point as the experimental data. Qualitative agreement between this model and the full SMC data is quite good, with all of the structure in the DCSs reproduced in detail at all energies considered. It may be noted that both models capture the first few interference features in the near-forward direction. The IAM would be expected to be most successful at small

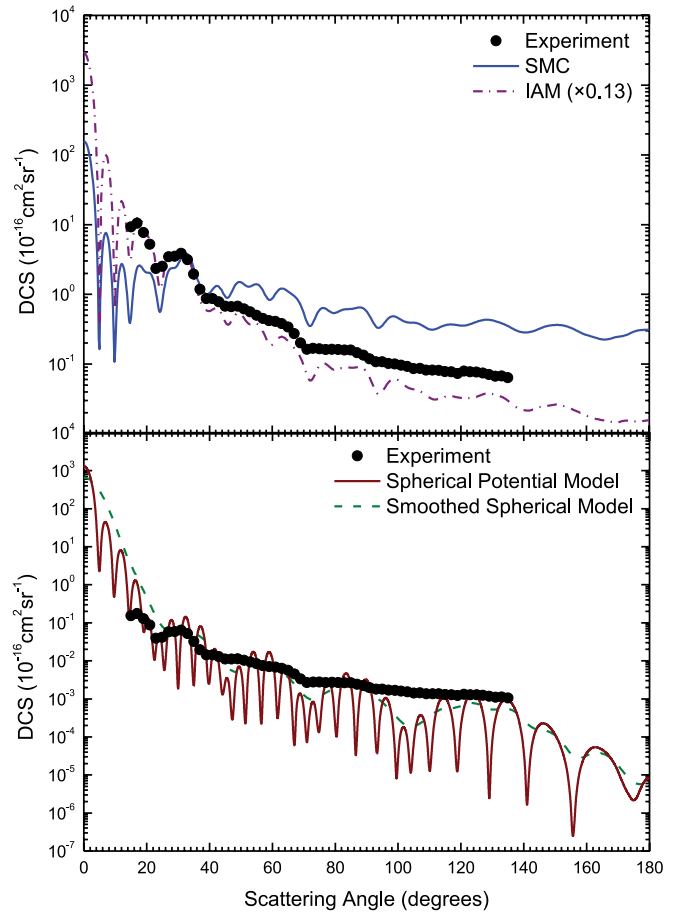


FIG. 5. (Color online) As for Fig. 3, but at an incident energy of 400 eV.

scattering angles [see Eq. (1)], as interference at the smallest momentum transfers is associated with the largest internuclear spacings, which are here given by the diameter of C_{60} (711 pm [26]). It is also worth noting that the Born cross section for the carbon atom is a monotonically decreasing function of θ ; therefore any structure in the C_{60} DCS produced by this model must come from $A(\mathbf{q})$, a term that represents the relative geometry of the scattering centers and thus builds interference effects into the cross section. Therefore, that the IAM model predicts the same oscillatory structure in the DCS as the full SMC calculation is a strong indication that the oscillatory structure in the DCS is largely described by interference due to diffraction effects.

Qualitatively, the IAM shows an excellent description of the forward scattering, with this model and the experimental data both showing a more strongly forward peaked cross section than the full SMC calculation. At incident energies 300 eV and lower, the IAM decreases more rapidly than either the experimental data or SMC results. In part, this is doubtless because these energies, where the de Broglie wavelength is much longer than the internuclear separations, are too low for either the Born or the independent-atom approximations to be fully valid. As the incident energy is raised, the agreement between the IAM and the experimental results steadily improves and is excellent by 500 eV, over the entire angular range.

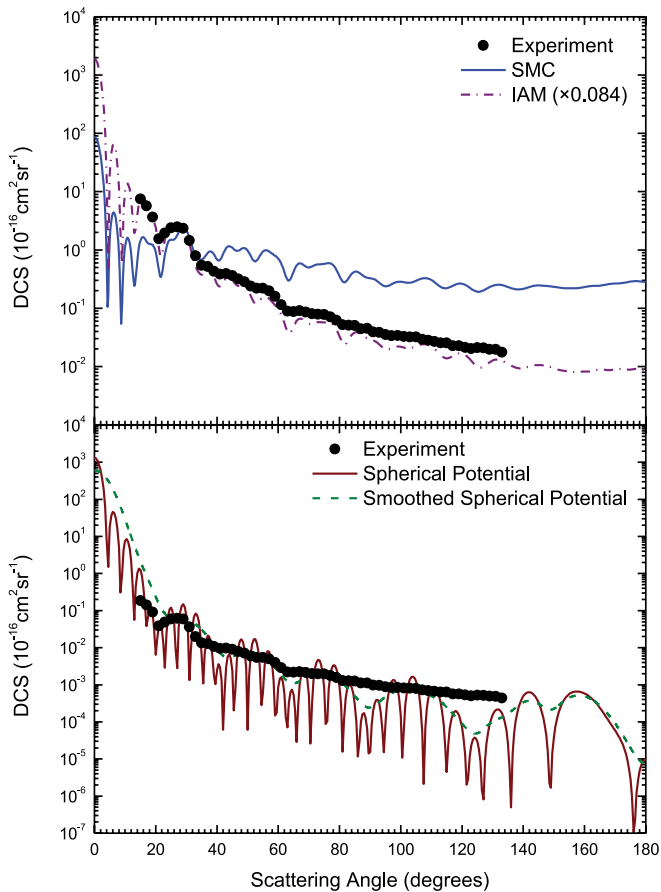


FIG. 6. (Color online) As for Fig. 3, but at an incident energy of 500 eV.

The good agreement between the IAM and experimental results is, in fact, quite remarkable considering the energies involved in the present study. A similar IAM was employed by Hedberg *et al.* [26] to interpret electron diffraction patterns and hence measure the bond lengths in C_{60} . Electron energies in diffraction experiments are typically of the order of several tens of keV, such that the de Broglie wavelength of the incident electron is much shorter (typically 10 pm or less) than the shortest interatomic spacing (140 pm [26]). The IAM would be expected to be most successful at these high scattering energies where diffraction effects are most pronounced. Here the electron wavelength is somewhat longer than in this regime, yet this simple interference model still provides an excellent account of both the diffraction structure and the overall distribution of the measured cross sections.

At the highest energies considered here, each of the simple models has an overall angular dependence closer to that of the measured DCS than does the SMC result calculated in the static-exchange approximation. Comparison with the independent-atom model, in particular, indicates that by 500 eV, the measured DCS exhibits the q^{-4} dependence on the momentum transfer characteristic of the Born approximation, while the SMC results vary much more slowly with the scattering angle. The Born approximation does, however, have a well-known tendency to overestimate contributions from low partial waves, leading to cross sections that are too

large at intermediate electron energies [27]. For this reason, the IAM is not recommended for normalizing the present measurements, in spite of the good qualitative agreement at the higher energies.

In previous studies of elastic electron scattering by smaller molecules, where it has been possible to compare to absolute measurements, it has generally been found that single-channel calculations with both the SMC and other methods tend to overestimate scattering at intermediate and high angles for impact energies above approximately 15 eV. Cho, Lee, and co-workers [28–32] have shown that including an absorbing potential in their iterative-Schwinger procedure to account for flux loss to inelastic (electronic excitation and, especially, ionization) channels greatly improves the angular dependence in this intermediate-energy region. The inclusion of coupling to inelastic channels may therefore be expected to improve the performance of the SMC method at higher energies in the present case; however, two considerations argue against this view. First, the shape of the SMC DCSs for C_{60} agrees quite well with the present measurements at 100 and 150 eV, in the energy range where the electron-impact ionization cross section of C_{60} is maximal [33,34]. Second, the spherical-shell and independent-atom and Born models also neglect inelastic channels, yet each describes the fall-off of the DCS with angle at the higher energies better than the SMC calculation. Further study of this aspect of the problem is warranted. At present, we note that the SMC method appears to provide a good description of the scattering up to about 150 eV and therefore should provide a reasonably accurate normalization for the experimental data. At higher energies, the correct normalization is more doubtful, given the limitations of each theoretical approach.

V. CONCLUSIONS

Differential cross sections for electron scattering by C_{60} in the 100 to 500 eV energy range have been measured and calculated from first principles. The experimental and theoretical DCSs are in overall good agreement at 100 and 150 eV. At 200 eV and above, agreement on the interference features remains good, but the measured DCS falls off more quickly with increasing scattering angle than predicted by the full SMC calculation. A simpler independent-atom model shows the reverse trend, with increasingly good agreement with experiment as the incident energy is raised. All of the structure observed in the DCSs appears to be accounted for by interference, as demonstrated by the success of an independent-atom scattering model in reproducing that structure.

ACKNOWLEDGMENTS

L.R.H. and B.L. acknowledge funding of this research by the Australian Research Council, under its Centre of Excellence program. The work of C.W. and V.M. was supported by the Chemical Sciences, Geosciences, and Biosciences Division, Office of Basic Energy Sciences, Office of Science, US Department of Energy, and made use of the Jet Propulsion Laboratory's Supercomputing and Visualization Facility.

- [1] V. Tarnovskiy, H. Duetsch, S. Matt, T. D. Märk, R. Basner, M. Schmidt and K. Becker, in *Proceedings of the Eighth International Symposium on Gaseous Electronics*, edited by L. G. Christophorou and J. K. Olthaff (Kluwer, Dordrecht, 1998).
- [2] W. Keller and M. A. Coplan, *Chem. Phys. Lett.* **193**, 89 (1992).
- [3] O. Elhamidi, J. Pommier, and R. Abouaf, *J. Phys. B: At. Mol. Opt. Phys.* **30**, 4633 (1997).
- [4] M. Lezius, P. Scheier, and T. D. Märk, *Chem. Phys. Lett.* **203**, 232 (1993).
- [5] D. Smith, P. Španěl, and T. D. Märk, *Chem. Phys. Lett.* **213**, 202 (1993).
- [6] D. Smith and P. Španěl, *J. Phys. B: At. Mol. Opt. Phys.* **29**, 5199 (1996).
- [7] O. Elhamidi, J. Pommier, and R. Abouaf, *J. Phys. B: At. Mol. Opt. Phys.* **30**, 4633 (1997).
- [8] M. Lezius, P. Scheier, and T. D. Märk, *Chem. Phys. Lett.* **203**, 232 (1993).
- [9] T. Jaffke, E. Illenberger, M. Lezius, Š. Matejčík, D. Smith, and T. D. Märk, *Chem. Phys. Lett.* **226**, 213 (1994).
- [10] V. Tarnovsky, P. Kurunczi, S. Matt, T. D. Märk, H. Duetsch, and K. Becker, *J. Phys. B: At. Mol. Opt. Phys.* **31**, 3043 (1998).
- [11] H. Duetsch, K. Becker, and T. D. Märk, *J. Phys. B: At. Mol. Opt. Phys.* **29**, 5175 (1996).
- [12] S. Keller, E. Engel, H. Ast, and R. M. Dreizler, *J. Phys. B: At. Mol. Opt. Phys.* **30**, L703 (1997).
- [13] S. Keller and E. Engel, *Chem. Phys. Lett.* **299**, 165 (1999).
- [14] O. Kidun and J. Berakdar, *Philos. Mag.* **86**, 2529 (2006).
- [15] H. Tanaka, L. Boesten, K. Onda, and O. Ohashi, *J. Phys. Soc. Jpn.* **63**, 485 (1994).
- [16] Yu. S. Gordeev, V. M. Mikoushkin, and V. V. Shnitov, *Mol. Mater.* **13**, 1 (2000).
- [17] L. G. Gerchikov, P. V. Efimov, V. M. Mikoushkin, and A. V. Solov'yov, *Phys. Rev. Lett.* **81**, 2707 (1998).
- [18] L. G. Gerchikov, A. V. Solov'yov, J.-P. Connerade, and W. Greiner, *J. Phys. B: At. Mol. Opt. Phys.* **30**, 4133 (1997).
- [19] R. R. Lucchese, F. A. Gianturco, and N. Sanna, *Chem. Phys. Lett.* **305**, 413 (1999).
- [20] F. A. Gianturco, R. R. Lucchese, and N. Sanna, *J. Phys. B: At. Mol. Opt. Phys.* **32**, 2181 (1999).
- [21] F. A. Gianturco and R. R. Lucchese, *J. Chem. Phys.* **111**, 6769 (1999).
- [22] C. Winstead and V. McKoy, *Phys. Rev. A* **73** 012711 (2006).
- [23] M. A. Haynes and B. Lohmann, *J. Phys. B: At. Mol. Opt. Phys.* **33**, 4711 (2000).
- [24] L.-M. Peng, *Micron* **30**, 625 (1999).
- [25] J. C. Nickel, P. W. Zetner, G. Shen, and S. Trajmar, *J. Phys. E: Sci. Instrum.* **22**, 730 (1989).
- [26] K. Hedberg, L. Hedberg, D. S. Bethune, C. A. Brown, H. C. Dorn, R. D. Johnson, and M. De Vries, *Science* **254**, 410 (1991).
- [27] See, e.g., G. Garcia and F. Manero, *Phys. Rev. A* **53**, 250 (1996).
- [28] L. M. Brescansin, P. Rawat, I. Iga, M. G. P. Homem, M.-T. Lee, and L. E. Machado, *J. Phys. B: At. Mol. Opt. Phys.* **37**, 471 (2004).
- [29] H. Cho, R. P. McEachran, H. Tanaka, and S. J. Buckman, *J. Phys. B: At. Mol. Opt. Phys.* **37**, 4639 (2004).
- [30] H. Cho, R. P. McEachran, S. J. Buckman, D. M. Filipović, V. Pejčev, B. P. Marinković, A. D. Stauffer, and E. J. Jung, *J. Phys. B: At. Mol. Opt. Phys.* **39**, 3781 (2006).
- [31] H. Cho, Y. S. Park, E. A. y Castro, G. L. C. de Souza, I. Iga, L. E. Machado, L. M. Brescansin, and M.-T. Lee, *J. Phys. B: At. Mol. Opt. Phys.* **41**, 045203 (2008).
- [32] L. M. Brescansin, L. E. Machado, M.-T. Lee, H. Cho, and Y. S. Park, *J. Phys. B: At. Mol. Opt. Phys.* **41**, 185201 (2008).
- [33] B. Dünser, M. Lezius, P. Scheier, H. Deutsch, and T. D. Märk, *Phys. Rev. Lett.* **74**, 3364 (1995).
- [34] S. Matt, B. Dünser, M. Lezius, H. Deutsch, K. Becker, A. Stamatovic, P. Scheier, and T. D. Märk, *J. Chem. Phys.* **105**, 1880 (1996).